NADPH oxidase links endoplasmic reticulum stress, oxidative stress, and PKR activation to induce apoptosis

Gang Li,[1] Christopher Scull,[1] Lale Ozcan,[1] and Ira Tabas[1,2,3]

[1]Department of Medicine, [2]Department of Physiology and Cellular Biophysics, and [3]Department of Pathology and Cell Biology, Columbia University, New York, NY 10032

Endoplasmic reticulum (ER)–induced apoptosis and oxidative stress contribute to several chronic disease processes, yet molecular and cellular mechanisms linking ER stress and oxidative stress in the setting of apoptosis are poorly understood and infrequently explored in vivo. In this paper, we focus on a previously elucidated ER stress–apoptosis pathway whose molecular components have been identified and documented to cause apoptosis in vivo. We now show that nicotinamide adenine dinucleotide phosphate reduced oxidase (NOX) and NOX-mediated oxidative stress are induced by this pathway and that apoptosis is blocked by both genetic deletion of the NOX subunit NOX2 and by the antioxidant *N*-acetylcysteine. Unexpectedly, NOX and oxidative stress further amplify CCAAT/enhancer binding protein homologous protein (CHOP) induction through activation of the double-stranded RNA–dependent protein kinase (PKR). In vivo, NOX2 deficiency protects ER-stressed mice from renal cell CHOP induction and apoptosis and prevents renal dysfunction. These data provide new insight into how ER stress, oxidative stress, and PKR activation can be integrated to induce apoptosis in a pathophysiologically relevant manner.

Introduction

A common feature of many disease processes is pathological cell death leading to tissue dysfunction. Two processes that are becoming increasingly recognized as inducers of pathological cell death are ER and oxidative stress (Chandra et al., 2000; Kim et al., 2008). Many of the diseases that feature ER and oxidative stress are associated with aging and/or obesity, including diabetes, atherosclerosis, renal disease, and neurodegenerative disease, and are becoming epidemic among humans in modern day society (Martínez, 2006; Kregel and Zhang, 2007; Kim et al., 2008). Nonetheless, progress in translating this understanding into useful therapeutic strategies has been disappointing. As one example, there is good evidence that the clinical progression of advanced atherosclerosis involves both ER and oxidative stress (Glass and Witztum, 2001; Tabas, 2010). However, ER stress involves many signaling pathways with differing pathological and physiological functions (Malhotra and Kaufman, 2007b; Ron and Walter, 2007), which makes targeting this process for atherosclerosis complex and challenging. Likewise, there are many sources of cellular oxidative stress in atherosclerotic lesional cells, and human trials using vitamin E as an antioxidant have failed to suppress the incidence of cardiovascular disease (Kris-Etherton et al., 2004; Williams and Fisher, 2005). Similar issues exist with other diseases driven by ER stress–induced apoptosis and oxidative stress.

An important approach to this problem is to gain a more in-depth understanding about molecular and cellular mechanisms and links between ER stress and oxidative stress, particularly in the process of cell death and in settings relevant to disease processes (Malhotra and Kaufman, 2007a). In this study, we

Correspondence to Ira Tabas: iat1@columbia.edu

Abbreviations used in this paper: CaMKII, calcium/calmodulin-dependent protein kinase II; CHOP, CCAAT/enhancer binding protein homologous protein; CMXRos, chloromethyl-X-rosamine; DCF, dihydrodichlorofluorescein; DHE, dihydroethidium; GAPDH, glyceraldehyde 3-phosphate dehydrogenase; IICR, IP3-induced calcium release; IP3, inositol 1,4,5-triphosphate; IP3R, IP3 receptor; LDL, low-density lipoprotein; NAC, *N*-acetylcysteine; NOX, NADPH oxidase; P-eIFα, phospho-eIF2α; PERK, PKR-like ER kinase; QPCR, quantitative PCR; TMR, tetramethylrhodamine; UPR, unfolded protein response; WT, wild type.

The Rockefeller University Press $30.00
J. Cell Biol. Vol. 191 No. 6 1113–1125
www.jcb.org/cgi/doi/10.1083/jcb.201006121

investigate these mechanisms using cultured macrophages as an in vitro model and the kidney in ER-stressed mice as an in vivo model. The macrophage model is relevant to advanced atherosclerosis (Tabas, 2010), and the kidney model is relevant to several renal diseases (Kitamura, 2008). With regard to macrophages, ER stress, often in combination with other proapoptotic hits, leads to apoptosis in part through the ER stress effector CCAAT/enhancer binding protein homologous protein (CHOP; Feng et al., 2003a; Thorp et al., 2009; Tabas, 2010). An important mechanism linking CHOP with apoptosis involves induction of the ER oxidase ERO1α, which causes activation of the ER calcium channel inositol 1,4,5-triphosphate (IP3) receptor (IP3R) and release of ER calcium (Li et al., 2009). The released calcium activates the enzyme calcium/calmodulin-dependent protein kinase II (CaMKII), which triggers both death receptor and mitochondrial pathways of apoptosis (Timmins et al., 2009). Oxidative stress can also be a trigger for apoptosis in macrophages, although the detailed molecular mechanisms are not well understood (Forman and Torres, 2002). There is evidence that ER stress–induced macrophage apoptosis occurs in advanced atherosclerosis and contributes to plaque necrosis, a critical process in atherothrombotic vascular disease (Feng et al., 2003b; Thorp et al., 2009; Tabas, 2010). Oxidative stress has also been implicated in atherosclerosis, but its importance in advanced lesional macrophage death and plaque necrosis is not known (Glass and Witztum, 2001; Bonomini et al., 2008). With regard to the renal model, several different inducers of renal dysfunction result in ER stress–induced apoptosis of renal tubular epithelial cells, podocytes, and other cells in the kidney (Kitamura, 2008). Renal disease can also be associated with oxidative stress (Locatelli et al., 2003), but, as mentioned above, its possible links to ER stress are not known.

Using these two models, we show here that the aforementioned branch of ER stress signaling involving calcium and CaMKII induces NADPH oxidase (NOX) and oxidative stress, which are necessary for ER stress–induced apoptosis. We also provide evidence that CHOP is amplified by NOX/oxidative stress–mediated activation of a double-stranded RNA–dependent protein kinase (PKR)–CHOP pathway and that this amplification pathway is important for the final apoptotic response.

Results

ER stress stimulates oxidative stress in macrophages, which is dependent on CHOP, proapoptotic calcium signaling, and NOX

Using two atherosclerosis-relevant inducers of ER stress, cholesterol loading and 7-ketocholesterol (Tabas, 2002; Myoishi et al., 2007), we determined whether oxidative stress was part of the previously elucidated CHOP–calcium–CaMKII pathway of apoptosis (Li et al., 2009; Timmins et al., 2009). Dihydrodichlorofluorescein (DCF) staining was used as a measure of intracellular peroxide accumulation (Wolber et al., 1987). We found that both inducers caused a substantial increase in the percentage of DCF-positive cells in wild-type (WT) macrophages, and the increase was much less in *Chop*$^{-/-}$ macrophages (Fig. 1 A). We next examined the calcium arm of the pathway using the intracellular calcium chelator BAPTA-AM. The increase in DCF-positive cells was decreased substantially by the chelator, which paralleled its inhibitory effect on annexin V staining as a measure of apoptosis (Fig. 1 B). DCF positivity and annexin V staining were also blocked by the CaMKII inhibitor KN93 but not by the structurally related inactive homologue KN92 (Fig. 1 C). We also used RNAi to silence CaMKII-γ, which is the isoform expressed in macrophages (Timmins et al., 2009). Two separate *Camk2g* siRNAs, which decrease *Camk2g* by ∼60 and 75% (Timmins et al., 2009), gave similar results as KN93 (Fig. 1 D). Thus, oxidative stress, like apoptosis, is stimulated by ER stress in macrophages and is dependent on CHOP, intracellular calcium, and CaMKII.

One well-documented source of oxidative stress in macrophages is NOX (Iles and Forman, 2002). To test the relevance of NOX in ER-stressed macrophages, we first determined whether expression of the major NOX isoform in macrophages, NOX2, was affected by ER stress. We found that both cholesterol loading and 7-ketocholesterol induced *Nox2* mRNA (Fig. 2 A, black bars). To test the causative role of NOX2 in oxidative stress and annexin V staining, we used siRNA against *Nox2*, which was effective in decreasing the mRNA to non–ER stress levels in the cholesterol- and 7-ketocholesterol–treated cells (Fig. 2 A, gray bars). This level of *Nox2* suppression significantly decreased both DCF staining and annexin V staining in ER-stressed macrophages (Fig. 2 B). As an independent approach, we compared macrophages isolated from WT versus *Nox2*$^{-/-}$ mice and found similar effects on oxidative stress and apoptosis, using either annexin staining or TUNEL for the apoptosis assay (Fig. 2, C and D). These data indicate that NOX plays an important role in the oxidative stress and apoptotic responses of macrophages subjected to ER stress.

The role of both CaMKII and NOX in ER stress–induced oxidative stress and apoptosis raised the question as to whether the two enzymes were in the same or different pathways. Consistent with their being in the same pathway, inhibition of CaMKII activity with KN93, or genetic targeting of the kinase through the use of *Camk2g*$^{-/-}$ macrophages, blocked *Nox2* mRNA induction by cholesterol loading or 7-ketocholesterol (Fig. 3 A). We showed previously that CaMKII activation requires an ERO1α–IP3R1–calcium release pathway (Li et al., 2009), which predicts that IP3R1 and ERO1α would play a role in *Nox2* induction. For this purpose, we transfected macrophages with an *Ero1a* siRNA that decreases ERO1α expression by ∼50% or an *Ip3r1* siRNA that decreases IP3R1 expression by ∼60% compared with scrambled RNA (Li et al., 2009) and found that each was able to suppress *Nox2* mRNA induction (Fig. 3, B and C).

Our previous work showed that a key downstream effector of CaMKII-induced apoptosis is the mitogen-activated protein kinase JNK (Timmins et al., 2009). We found here that the JNK inhibitor SP600125 blocked *Nox2* mRNA induction, DCF positivity, and annexin V staining in ER-stressed macrophages (Fig. 3, D and E). The *Nox2* mRNA data were confirmed using macrophages from *Jnk2*$^{-/-}$ mice (Fig. 3 D, right graph). In summary, the data in Figs. 1–3 suggest that NOX plays a critical yet previously

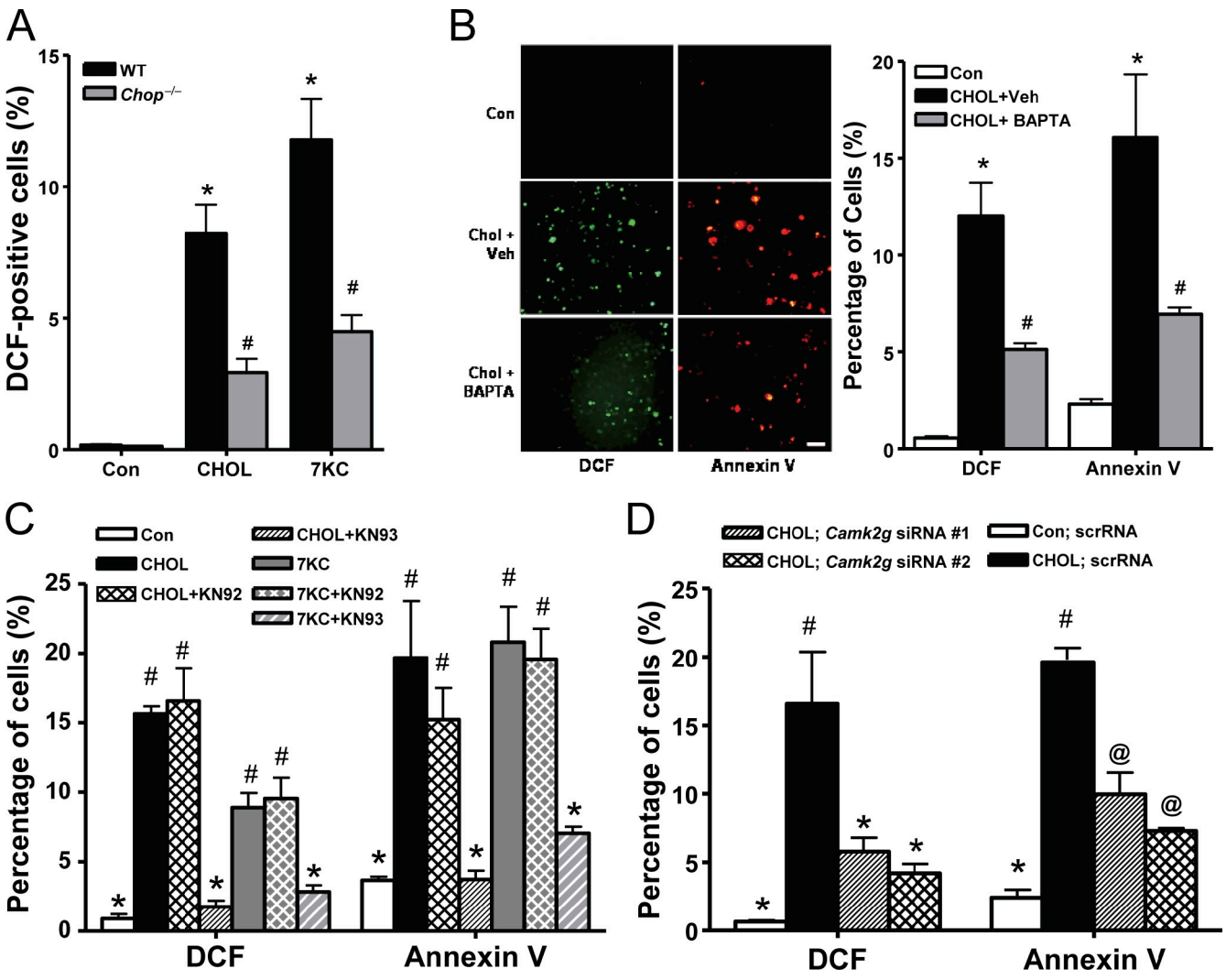

Figure 1. **ER-stressed macrophages undergo oxidative stress, which is dependent on CHOP, calcium, and CaMKII.** (A) Peritoneal macrophages from *Chop*$^{+/+}$ (WT) and *Chop*$^{-/-}$ mice were incubated for 15 h without sterol (Con), under cholesterol-loading conditions (CHOL), or with 7-ketocholesterol (7KC). Intracellular peroxide accumulation was then assayed by DCF fluorescence. Three fields for each sample were quantified and expressed as a percentage of DCF-positive cells. (B) Macrophages were pretreated for 1 h with 5 µM BAPTA-AM or with equivalent volumes of vehicle (Veh). The cells were then incubated for 15 h under control or cholesterol-loading conditions and also with BAPTA-AM or vehicle control as indicated. Intracellular peroxide accumulation and apoptosis were assayed by DCF fluorescence (green) and Alexa Fluor 594–conjugated annexin V (red), respectively. Bar, 20 µm. (C) Macrophages were pretreated for 1 h in the absence or presence of 5 µM of the CaMKII inhibitor KN93 or the inactive analogue KN92, followed by incubation for 14 h without sterol under cholesterol-loading conditions or with 7-ketocholesterol. DCF fluorescence and annexin V staining were then assayed. (D) Macrophages were transfected with two different *Camk2g* siRNA constructs. After 72 h, the cells were incubated for 30 h under control or cholesterol-loading conditions and then assayed for DCF fluorescence and annexin V staining. Bars with the same symbols are not significantly different from each other, whereas bars with different symbols are significantly different from each other. $n = 3$ for each experimental group. scrRNA, scrambled RNA. Data are presented as means ± SEM.

unknown role in the ER stress–CHOP–calcium–CaMKII–JNK pathway of apoptosis.

Evidence for CHOP amplification through NOX/oxidative stress–mediated activation of PKR

The simplest way to integrate our previous findings (Li et al., 2009; Timmins et al., 2009) with the new data described thus far would be a linear pathway in which CHOP and CaMKII are upstream of NOX as follows: ER stress→CHOP→IP3R activation→ER calcium release→CaMKII activation→NOX activation→oxidative stress. However, the possibility of a bidirectional pathway was suggested by surprising data showing that absence of NOX2 actually suppressed both CaMKII activation/phosphorylation and CHOP induction in cholesterol-loaded or 7-ketocholesterol–treated macrophages (Fig. 4 A). Note that the transcriptional inducer of CHOP in the phospho-eIF2α (P-eIFα) pathway, ATF4, was also suppressed in *Nox2*$^{-/-}$ macrophages, whereas neither phospho–PKR-like ER kinase (PERK) nor *Xbp1* splicing was suppressed in *Nox2*$^{-/-}$ macrophages (Fig. 4, A and B). These data are consistent with the conclusion that NOX2 deficiency was specifically suppressing a non-PERK–activated P-eIF2α pathway rather than global ER stress. We therefore looked at another eIF2α kinase, PKR, and found that phosphorylation of this kinase, which is a measure of its activation, was substantially suppressed in *Nox2*$^{-/-}$ macrophages (Fig. 4 A).

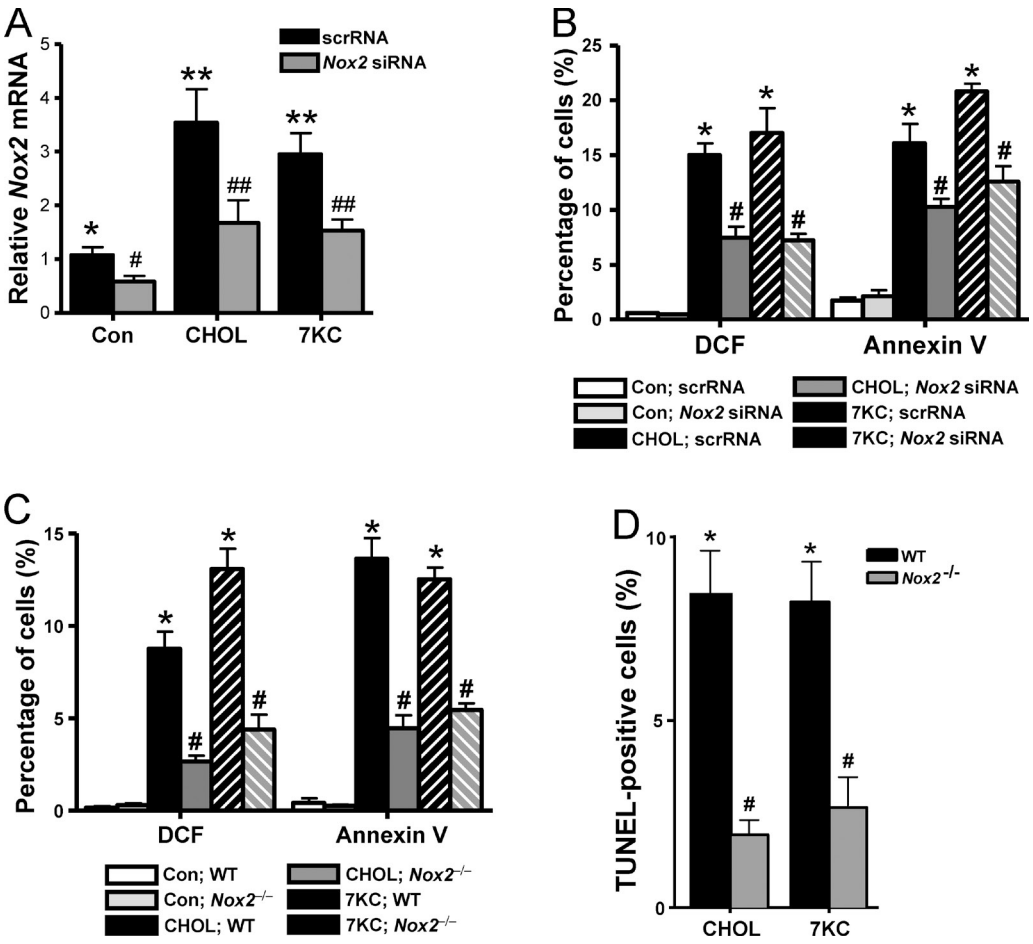

Figure 2. **Oxidative stress and apoptosis in ER-stressed macrophages are dependent on NOX2.** (A and B) Macrophages were transfected with *Nox2* siRNA and, after 72 h, were incubated without sterol (Con), under cholesterol-loading conditions (CHOL), or with 7-ketocholesterol (7KC). The cells were assayed for *Nox2* mRNA by RT-QPCR after 8 h (A) and DCF fluorescence and annexin V staining after 30 h (B). (C) Macrophages from WT or *Nox2*$^{-/-}$ mice were incubated for 14 h without sterol, under cholesterol-loading conditions, or with 7-ketocholesterol and then assayed for DCF and annexin V staining. (D) Macrophages from WT or *Nox2*$^{-/-}$ mice were incubated under cholesterol-loading conditions for 24 h or with 7-ketocholesterol for 20 h and then assayed for apoptosis by TUNEL staining. Bars with the same symbols are not significantly different from each other, whereas bars with different symbols are significantly different from each other. scrRNA, scrambled RNA. $n = 3$ for each experimental group. Data are presented as means ± SEM.

These data raised the possibility that NOX, through activation of PKR–P-eIF2α signaling, might amplify CHOP signaling and thus be necessary not only for CaMKII activation (Fig. 1, C and D) but also for induction of *Nox2* itself (i.e., positive feedback loop), oxidative stress, and, most importantly, apoptosis. To explore this possibility, we conducted a series of experiments using *Pkr* siRNA. As shown in Fig. 4 C, the siRNA was effective in suppressing PKR, and this was associated with suppression of P-eIF2α and CHOP. Moreover, *Pkr* siRNA was able to block the ER stress–induced increment in Nox2 induction (Fig. 4 D).

In terms of apoptosis, we first asked whether the partial suppression of CHOP seen in *Nox2*$^{-/-}$ macrophages (Fig. 4 A) would be enough to decrease apoptosis. We therefore looked at apoptosis in *Chop*$^{+/-}$ macrophages, which express ∼50% of the level of CHOP seen in WT macrophages (not depicted), and found that annexin V staining was indeed partially suppressed (Fig. 4 E, left). To test links among PKR, oxidative stress, and apoptosis, we tested the effect of *Pkr* siRNA on DCF fluorescence and annexin V staining. We found that both endpoints were significantly decreased in the siRNA-treated macrophages (Fig. 4 E, right). Finally, we reasoned that a mechanism by which NOX2 activated PKR might be oxidative stress. In support of this idea, we found that the increases in both phospho-PKR and CHOP were also partially suppressed by the antioxidant *N*-acetylcysteine (NAC; Fig. 4 F). These data provide strong support for the concept that NOX2-induced oxidative stress amplifies CHOP expression through PKR activation and that this process is important for the induction of *Nox2* itself as well as for oxidative stress and apoptosis.

NOX is necessary for activation of IP3R and the mitochondrial pathway of apoptosis in ER-stressed macrophages

The fact that CaMKII activation was suppressed in *Nox2*$^{-/-}$ cells (Fig. 4 A) suggested that NOX2 might be important in a key process upstream of CaMKII, IP3R activation (Li et al., 2009), as well an important proapoptotic process downstream of CaMKII, activation of the mitochondrial pathway of apoptosis (Timmins et al., 2009). To test the first prediction, we conducted

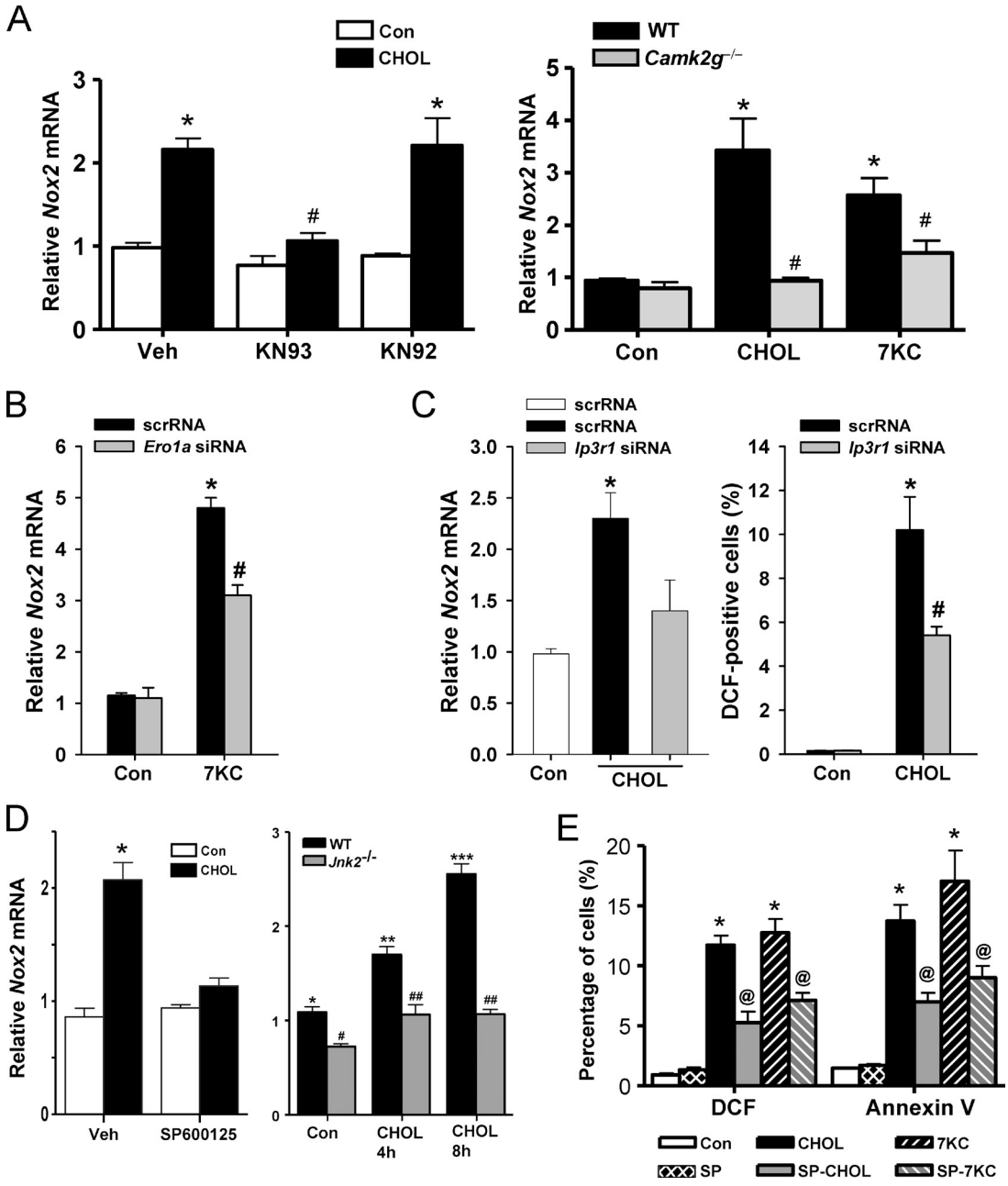

Figure 3. ***Nox2* induction by ER stress is dependent on CaMKII, ERO1α, IP3R1, and JNK.** (A, left) Macrophages were pretreated for 1 h in the absence or presence of 5 μM of the CaMKII inhibitor KN93, the inactive analogue KN92, or vehicle control (Veh), followed by incubation for 8 h without sterol (Con) or under cholesterol-loading conditions (CHOL). *Nox2* mRNA was then measured by RT-QPCR. (A, right) Peritoneal macrophages from WT or *Camk2g*$^{-/-}$ mice were incubated for 8 h without sterol, under cholesterol-loading conditions, or with 7-ketocholesterol (7KC) and then assayed for *Nox2* mRNA. (B) Macrophages were transfected with scrambled RNA (scrRNA) or *Ero1a* siRNA, which, after 72 h, led to an ~50% decrease in ERO1α expression as assessed by immunoblotting (Li et al., 2009). The cells were then incubated an additional 8 h without sterol or with 7-ketocholesterol and then assayed for *Nox2* mRNA. (C) Macrophages were transfected with scrambled RNA or *Ip3r1* siRNA. After 72 h, IP3R1 expression was decreased by 60% as assessed by immunoblotting (Li et al., 2009). The cells were then incubated without sterol or under cholesterol-loading conditions for an additional 8 or 30 h and then assayed for *Nox2* mRNA or DCF fluorescence, respectively. (D, left) Macrophages were pretreated for 1 h with 10 μM of the JNK inhibitor SP600125 or vehicle control and then incubated for 8 h without sterol or under cholesterol-loading conditions, also in the absence or presence of SP600125. (D, right) WT or Jnk2$^{-/-}$ macrophages were incubated under control conditions or for 4 or 8 h under cholesterol-loading conditions. *Nox2* mRNA was then assayed. (E) Macrophages were pretreated for 1 h with the JNK inhibitor SP600125 (SP) or vehicle control and then incubated for 15 h without sterol, under cholesterol-loading conditions, or with 7-ketocholesterol, also in the absence or presence of SP600125. DCF fluorescence and annexin V staining were then assayed. Bars with the same symbols are not significantly different from each other, whereas bars with different symbols are significantly different from each other. $n = 3$ for each experimental group. Data are presented as means ± SEM.

a standard intact-cell IP3R assay in which IP3-induced calcium release (IICR) is assayed at a given time point after exposure to a stimulus, in this case 6 h of cholesterol loading, using the ATP–purinergic receptor pathway as a tool to acutely generate IP3 (Charest et al., 1985). As we previously reported (Li et al., 2009), IICR was increased by cholesterol loading in

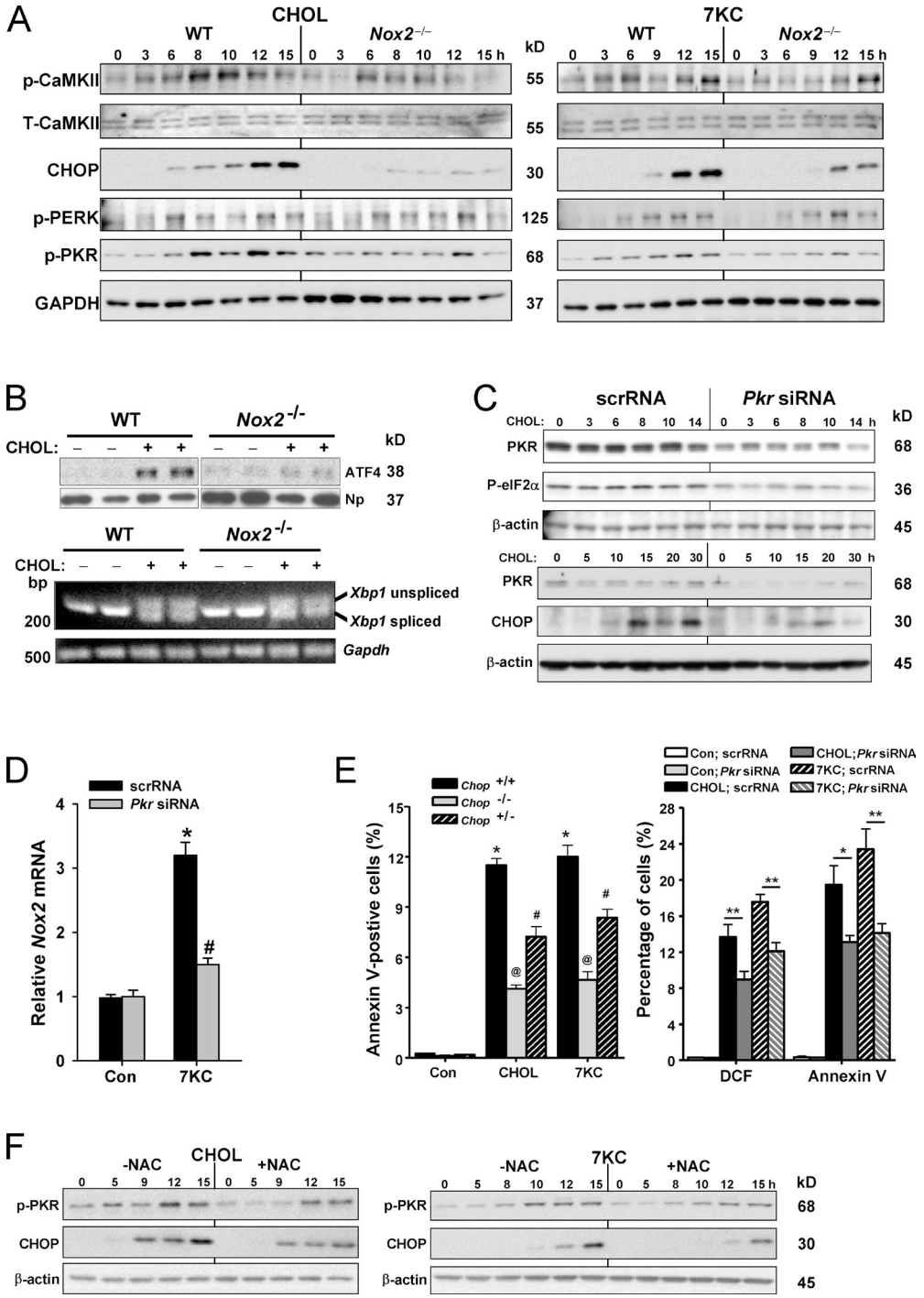

Figure 4. **Evidence for CHOP amplification through NOX/oxidative stress–mediated activation of PKR.** (A) Macrophages from WT or *Nox2*$^{-/-}$ mice were incubated under cholesterol-loading conditions (CHOL) or with 7-ketocholesterol (7KC) for the indicated times. Lysates were then immunoblotted for phospho-CaMKII (p-CaMKII), total CaMKII (T-CaMKII), CHOP, phospho-PERK (p-PERK), phospho-PKR (p-PKR), and GAPDH. (B) Macrophages from WT or *Nox2*$^{-/-}$ mice were incubated under cholesterol-loading conditions for 8 h (ATF4 experiment) or 9 h (XBP1 experiment). Nuclei were isolated and immunoblotted for ATF4 and nucleophosmin (Np) loading control, or RNA was extracted and assayed for spliced and unspliced *Xbp1* and *Gapdh* loading control. (C) Macrophages were transfected with scrambled RNA (scrRNA) or *Pkr* siRNA. After 72 h, the cells were incubated for the indicated times under cholesterol-loading conditions. Lysates were then immunoblotted for PKR, phospho-eIF2α (P-eIF2α), CHOP, and β-actin loading control. (D) Macrophages were transfected with scrambled RNA or *Pkr* siRNA. After 72 h, the cells were incubated for an additional 8 h without sterol (Con) or with 7-ketocholesterol and then assayed for *Nox2* mRNA. The data are displayed as *Nox2* mRNA levels relative to those for the control scrambled RNA group. (E, left) Macrophages from WT, *Chop*$^{+/-}$, or *Chop*$^{-/-}$ mice were incubated for 14 h without sterol, under cholesterol-loading conditions, or with 7-ketocholesterol and then assayed for annexin V staining. (E, right) Macrophages were transfected with scrambled RNA or *Pkr* siRNA. After 72 h, the cells were incubated for an additional 30 h without sterol, under cholesterol-loading conditions, or with 7-ketocholesterol and then assayed for DCF fluorescence and annexin V staining. In this graph, * indicates $P < 0.05$ and ** indicates $P < 0.01$. (F) Peritoneal macrophages were pretreated in the absence or presence of 5 μM of the antioxidant *N*-acetylcysteine (NAC). The cells were then incubated under cholesterol-loading conditions or with 7-ketocholesterol for the indicated time periods, also in the absence or presence of NAC. Lysates were then immunoblotted for phospho-PKR, CHOP, and β-actin. $n = 3$ for each experimental group. Data are presented as means ± SEM.

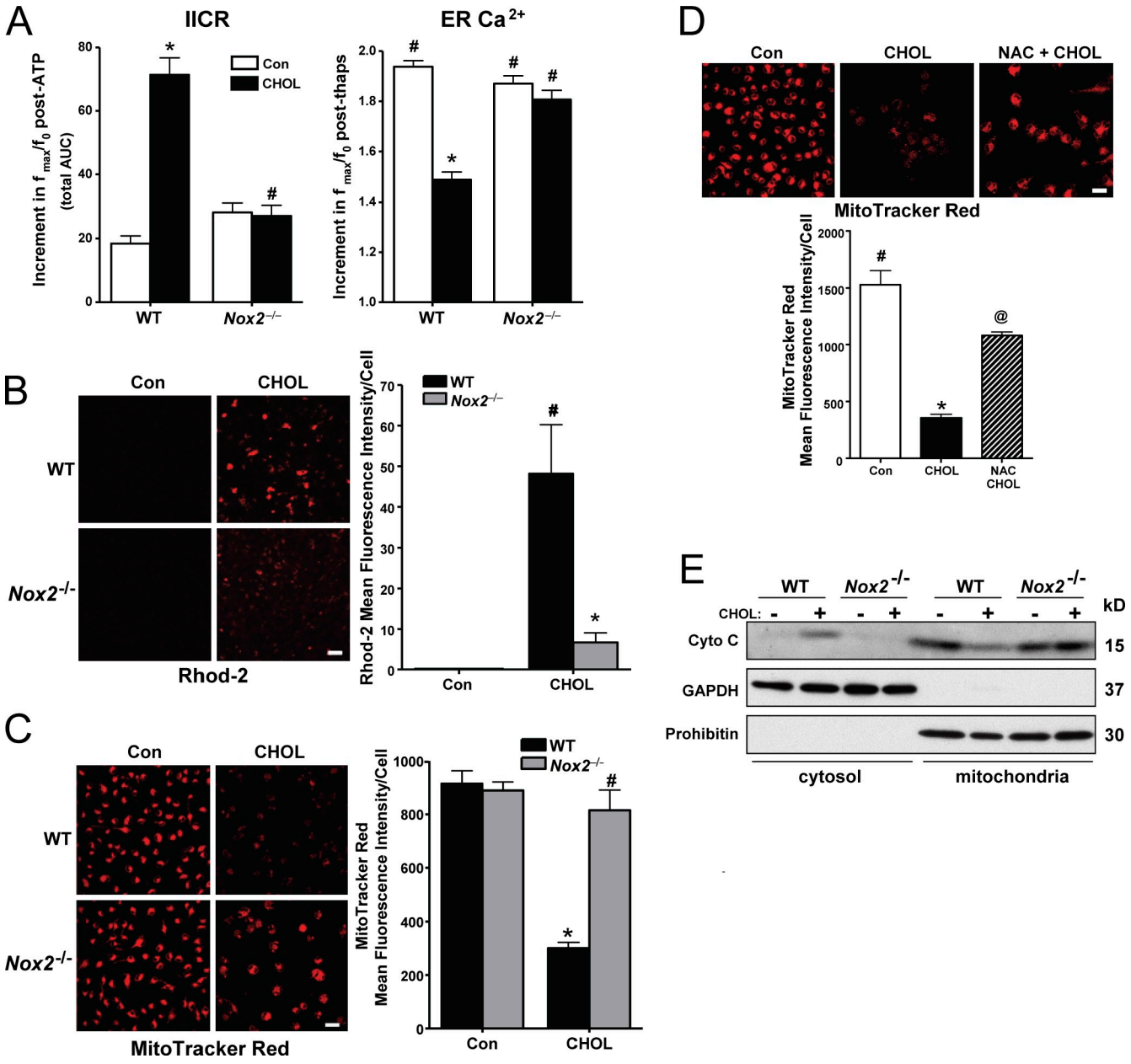

Figure 5. **NOX is necessary for activation of IP3R and the mitochondrial pathway of apoptosis in ER-stressed macrophages.** (A, left) Macrophages from WT or *Nox2*$^{-/-}$ mice were incubated for 6 h under cholesterol-loading conditions (CHOL) and then assayed for IICR, as reflected by the post-ATP increment in the area under curve for ATP-induced calcium release (n = 30 cells). (A, right) To assess ER luminal calcium stores, the cells were treated with 2 µM thapsigargin. The bar graph shows the mean peak amplitude of the postthapsigargin Fluo-3 response. (B) Macrophages from WT or *Nox2*$^{-/-}$ mice were incubated for 2 h under control (Con) or cholesterol-loading conditions. 10 µM Rhod-2 was then added to the media, and the cells were incubated on ice for 1 h at 4°C. Next, the cells were rinsed to remove extracellular Rhod-2 and incubated for an additional 5 h, also under control or cholesterol-loading conditions. At the end of the incubation period, the cells were visualized using confocal microscopy and imaged as described in Materials and methods. Fluorescence intensity for ~100 cells was measured for each treatment group. (C) Macrophages from WT or *Nox2*$^{-/-}$ mice were incubated for 14 h under control or cholesterol-loading conditions and then assayed for MitoTracker red staining as described in Materials and methods. (D) Macrophages were pretreated for 1 h with 0.5 µM NAC, followed by incubation under control or cholesterol-loading conditions for 14 h, also with or without NAC. The cells were then stained with MitoTracker red CMXRos and imaged and quantified as in C. (E) Macrophages from WT or *Nox2*$^{-/-}$ mice were incubated for 8 h under control or cholesterol-loading conditions. Cytosolic and mitochondrial fractions were assayed for cytochrome *c* (Cyto C), GAPDH (cytosolic marker), and prohibitin (mitochondrial marker). For all graphs, bars with the same symbols are not significantly different from each other, whereas bars with different symbols are significantly different from each other. n = 3 for each experimental group. Bars, 10 µm. Data are presented as means ± SEM.

WT macrophages (Fig. 5 A, left, left pair of bars). However, there was no increase in IICR in cholesterol-loaded *Nox2*$^{-/-}$ macrophages (Fig. 5 A, left, right pair of bars). In theory, these increases and decreases in IICR could simply be driven by increases and decreases in ER lumenal calcium, respectively, rather than by primary changes in IP3R activity. However, ER lumenal calcium, as assessed by measuring thapsigargin-releasable calcium, was lower in the high-IICR cholesterol-loaded WT macrophages and higher in the low-IICR *Nox2*$^{-/-}$ macrophages (Fig. 5 A, right). Thus, the changes in IICR seen in Fig. 5 A (left)

were caused by changes in the fraction of ER calcium being released via differential IP3R activation. These data provide evidence that NOX2 is necessary for IP3R-mediated calcium release, which is consistent with the finding that NOX amplifies CHOP signaling (Fig. 4 A) in the context of the previously described CHOP–ERO1α–IP3R pathway (Li et al., 2009).

A key proapoptotic process triggered by CaMKII activation is mitochondrial calcium accumulation and loss of mitochondrial membrane potential (Yao and Tabas, 2001; Timmins et al., 2009). To assess the role of NOX in these processes, we compared cholesterol-loaded WT and *Nox2*$^{-/-}$ macrophages for mitochondrial staining by Rhodamine-2 (Rhod-2) staining, a measure of mitochondrial calcium (Trollinger et al., 1997), and by MitoTracker red (chloromethyl-X-rosamine [CMXRos]), a measure of mitochondrial membrane potential (Poot et al., 1996). Cholesterol loading led to an increase in Rhod-2 staining in WT macrophages, and this was decreased substantially in *Nox2*$^{-/-}$ macrophages (Fig. 5 B). MitoTracker staining was diminished by cholesterol loading, which is consistent with its ability to cause mitochondrial membrane depolarization (Yao and Tabas, 2001), and this effect was also blocked in *Nox2*$^{-/-}$ macrophages (Fig. 5 C). The cholesterol-induced loss of MitoTracker red staining was also markedly prevented by NAC (Fig. 5 D). Mitochondrial membrane depolarization can lead to permeabilization of the outer mitochondrial membrane and release of proapoptotic factors, notably cytochrome *c* (Green and Reed, 1998). This process occurs in ER-stressed macrophages and is important for apoptosis (Yao and Tabas, 2001; Timmins et al., 2009). We show here that the increase in cytosolic cytochrome *c* and decrease in mitochondrial cytochrome *c* induced by cholesterol loading in WT macrophages were diminished in *Nox2*$^{-/-}$ macrophages (Fig. 5 E). Thus, activation of NOX plays an important role in the mitochondrial pathway of apoptosis in ER-stressed macrophages.

Functional role of NOX in ER stress–induced pathology in vivo

ER stress–induced macrophage apoptosis plays an important role in plaque necrosis in very advanced atherosclerosis, which in mouse models of atherosclerosis requires 4 mo or more of sustained hypercholesterolemia. However, *Nox2*$^{-/-}$ mice on either the *Apoe*$^{-/-}$ or *Ldlr*$^{-/-}$ backgrounds or in a bone marrow transplant model lose weight and become ill after 8 wk of hypercholesterolemia, likely because of infection (Pollock et al., 1995; unpublished data). Therefore, currently available genetic models cannot be used to assess the role of NOX in advanced atherosclerosis. Nonetheless, consistent with our in vitro data, we did find that atherosclerotic lesions from *Chop*$^{-/-}$;*Apoe*$^{-/-}$ mice, which are partially protected against advanced lesional macrophage apoptosis (Thorp et al., 2009), had 36% less dihydroethidium (DHE) staining as a measure of peroxide accumulation ($P < 0.05$; Laurindo et al., 2008) and 37% less *Nox2* mRNA, as assayed by laser capture microdissection/reverse transcription quantitative PCR (QPCR), compared with lesions from *Chop*$^{+/+}$;*Apoe*$^{-/-}$ ($P < 0.05$ for both endpoints; unpublished data).

To directly test the role of NOX2 in vivo, we used a short-term model of systemic ER stress that utilizes injection of subtoxic amounts of the unfolded protein response (UPR) activator tunicamycin and monitors effects on renal tubular epithelium, a pathophysiologically relevant site for ER stress–induced apoptosis and tissue dysfunction (Zinszner et al., 1998; Kitamura, 2008). In particular, ER stress–induced renal cell apoptosis is a common pathway in several renal diseases (Kitamura, 2008). To test the link between CaMKII and NOX2 expression, we immunostained kidney slices from ER-stressed WT and *Camk2g*$^{-/-}$ mice for NOX2 protein and stained them with DHE for evidence of superoxide accumulation. As with cultured macrophages, both NOX2 and DHE staining were increased in the setting of ER stress, and the ER stress–induced increment in both parameters was much lower in the absence of CaMKII-γ (Fig. 6, A and B). To examine apoptosis, we used the TUNEL stain and found that the kidney was markedly protected from ER stress–induced apoptosis in *Nox2*$^{-/-}$ mice (Fig. 6 C). Most importantly, *Nox2*$^{-/-}$ mice were protected against renal dysfunction, as measured by serum creatinine and urinary albumin (Fig. 6 D). Consistent with these data and the positive feedback cycle revealed in the cell culture experiments, the induction of CHOP in the kidney of ER-stressed WT mice was also blunted in *Nox2*$^{-/-}$ mice (Fig. 6 E). Thus, the key role of NOX in ER stress–induced apoptosis occurs and is functionally important in vivo.

Discussion

ER stress–induced apoptosis is a critical process in several widespread chronic disease processes (Kim et al., 2008), and although oxidative stress has been implicated as a proapoptotic process in ER stress–induced cell death, the source of oxidative stress and its molecular connections to ER stress represent major gaps in our knowledge in this area (Malhotra and Kaufman, 2007a). The data in this study address these gaps by showing that NOX and NOX-induced oxidative stress are triggered by a specific arm of ER stress signaling involving calcium and CaMKII, and the resulting oxidative stress participates in an amplification pathway involving the PKR–CHOP pathway. As such, a positive feedback loop results in which CHOP induces *Nox2* and NOX2 activates CHOP. However, a simple cycle involving all molecules in the pathway is not supported by our previous finding that silencing of ERO1α does not suppress CHOP (Li et al., 2009). Note that ERO1α and CHOP would be the two most separated points in a clockwise cycle because CHOP directly induces *Ero1a* to trigger the IP3R1–calcium–CaMKII–NOX2–apoptosis cascade (Li et al., 2009). Thus, there are many nodes between ERO1α and CHOP in the clockwise direction, and we reason that CHOP expression is likely maintained in ERO1α-silenced cells by one or more additional inputs in these areas.

The findings reported here raise new questions about signal transduction reactions downstream of the UPR and upstream of PKR. For example, with regard to *Nox2* induction, the data in Fig. 3 D raise the possibility that JNK may be a transcriptional activator of the *Nox2* gene. This hypothesis is consistent with a previous finding in smooth muscle cells that *Nox4*, another member of the NOX family, is induced by 7-ketocholesterol through an IRE1α–JNK pathway (Pedruzzi et al., 2004). In view of this work, we considered a role for NOX4-mediated oxidative stress

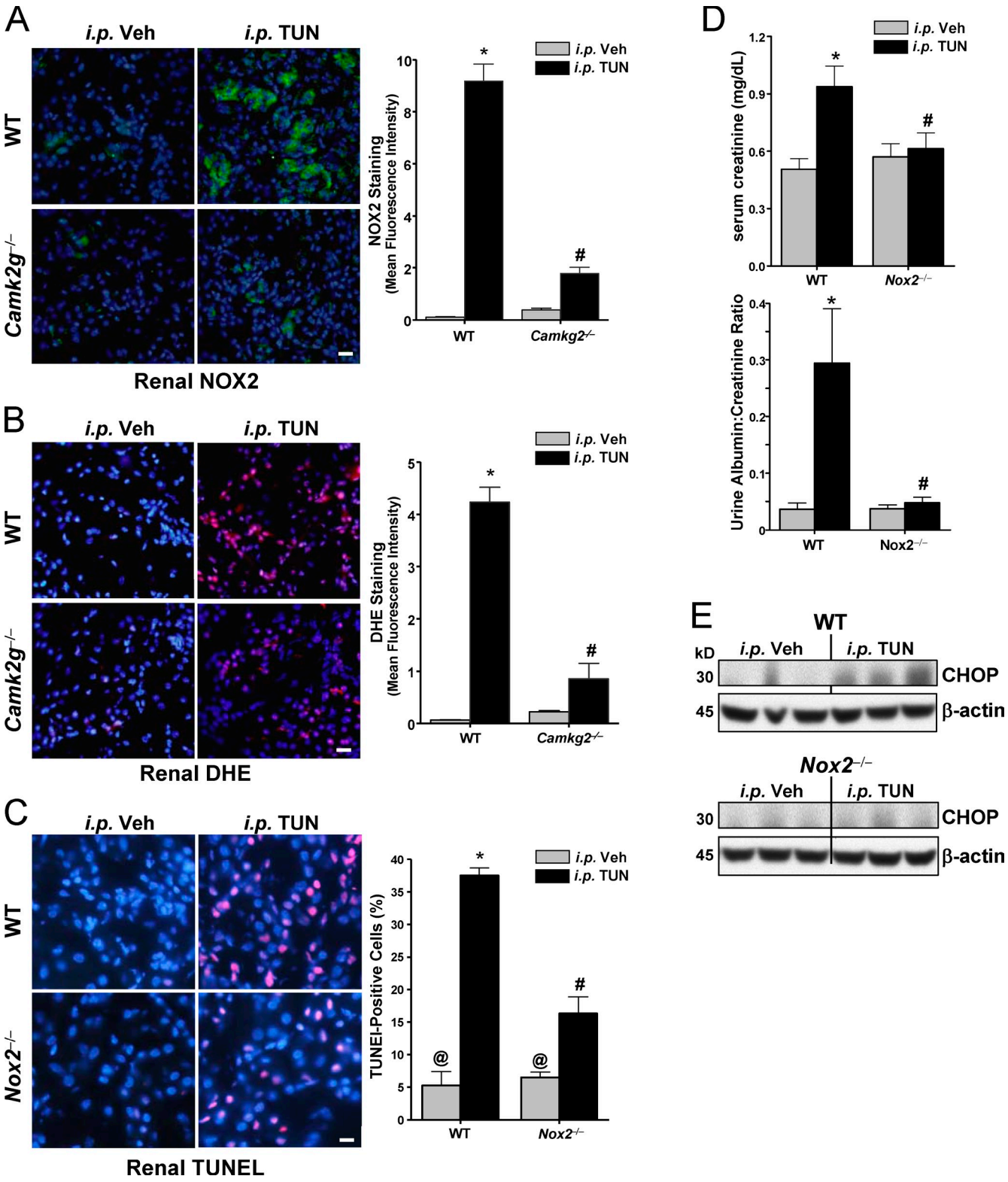

Figure 6. **NOX2 deficiency protects against ER stress–induced renal cell apoptosis, renal dysfunction, and CHOP induction.** (A–C) WT, *Camk2g*$^{-/-}$, and *Nox2*$^{-/-}$ mice were injected i.p. with 1 mg/kg tunicamycin (TUN) or vehicle (Veh) control. The kidneys were harvested 40 h later and stained using anti-NOX2 (A), DHE (superoxide accumulation; B), or TUNEL (apoptosis; C). All sections were also stained with DAPI to visualize nuclei. Bars, 20 μm. The bar graphs show quantification of the mean fluorescent intensities from three mice in each group. (D) Serum creatinine levels and urine albumin levels (normalized to urine creatinine) were determined for all groups of mice. (E) Kidney lysates were assayed for CHOP and β-actin by immunoblotting. For A–D, bars with the same symbols are not significantly different from each other, whereas bars with different symbols are significantly different from each other. $n = 3$ for each experimental group. Data are presented as means ± SEM.

in the pathway described here, but *Nox2* mRNA is far more abundant than *Nox4* mRNA in primary macrophages (unpublished data). In terms of PKR activation in our model, ER stress has been shown to activate a molecule called PKR-activating protein, leading to sustained PKR-mediated CHOP expression (Lee et al., 2007). In another setting, there is evidence of ER stress–induced PKR activation in the adipose and liver of obese mice (Nakamura et al., 2010), and although the mechanism has not been reported, it is intriguing to consider the separate finding that obese adipose tissue has increased expression of NOX and increased oxidative stress (Furukawa et al., 2004). In the model described here, oxidative stress plays a role in PKR activation (Fig. 4 F), and a previous study showed hydrogen peroxide treatment of Jurkat cells induces PKR through a pathway involving Janus kinase–signal transducer and activator of transcription signaling and interferon-γ induction (Pyo et al., 2008). Whether NOX is involved in any of these pathways remains to be explored.

We chose to use macrophages as a cell culture model to explore mechanisms linking ER stress and NOX because of pathophysiologic relevance in advanced atherosclerosis (Ibrahimi and Abumrad, 2002). There is also ample evidence of oxidative stress in advanced plaques (Bonomini et al., 2008), and the expression of NOX subunits, including NOX2, is up-regulated in atherosclerotic lesions (Sorescu et al., 2002). Moreover, we found that *Nox2* mRNA and DHE staining, a measure of superoxide accumulation, were lower in *Chop*$^{-/-}$ lesions (unpublished data), which was consistent with our data. Although there are several informative studies on early-to-mid–stage atherogenesis using *Nox2*-null mice (Hsich et al., 2000; Barry-Lane et al., 2001; Vendrov et al., 2007; Judkins et al., 2010), the endpoint in such studies—lesion area—is entirely different from the atherosclerosis endpoints relevant to the signaling pathways described here—advanced lesional macrophage apoptosis and plaque necrosis. Unfortunately, advanced atherosclerosis is not amenable to in vivo studies using *Nox2*-null mice because during the months it takes to develop very advanced lesions, the null mice lose weight and become ill (unpublished data) and have decreased plasma cholesterol and triglyceride (Kirk et al., 2000), which may be caused by infection (Pollock et al., 1995).

The ultimate goal of elucidating signaling pathways linked to pathophysiological processes is to suggest novel, mechanism-based approaches to disease prevention or treatment. Uninformed efforts at using antioxidant therapy in human diseases have been generally disappointing (e.g., the failure of vitamin E to prevent atherosclerotic heart disease; Williams and Fisher, 2005). However, understanding the interplay between ER stress and a specific cause of intracellular oxidative stress, as revealed here, could suggest new therapeutic strategies that are targeted, more specific, and mechanism based. In the case of the many disease processes involving both ER and oxidative stress, including advanced atherosclerosis and renal disease, our findings herein suggest that drugs targeting the CHOP branch of the UPR, and perhaps PKR in particular, and/or NOX may have particular promise. Conversely, attempts to kill cancerous cells can be thwarted by resistance to ER stress– and oxidative stress–induced apoptosis (Healy et al., 2009; Verrax et al., 2009), and knowledge of the pathways revealed here may suggest new mechanisms that could explain this resistance and new therapies for overcoming it.

Materials and methods

Reagents

Cell culture media and reagents were obtained from Invitrogen. HPLC-grade organic solvents were purchased from Thermo Fisher Scientific. Low-density lipoprotein (LDL; density, 1.020–1.063) was isolated from fresh human plasma by preparative ultracentrifugation as described previously (Havel et al., 1955). Our experiments with purchased human plasma were exempt from Institutional Review Board approval because the sources were anonymous. Acetyl-LDL was prepared by reaction of LDL with acetic anhydride (Basu et al., 1976). KN93 (2-[*N*-(2-hydroxyethyl)]-*N*-(4-methoxybenzenesulfonyl)amino-*N*-(4-chlorocinnamyl)-*N*-methylbenzylamine), KN92 ([*N*-(4-methoxybenzenesulfonyl)]amino-*N*-(4-chlorocinnamyl)-*N*-methylbenzylamine phosphate), and SP600125 (anthra(1,9-cd)pyrazol-6(2*H*)-1) were obtained from EMD. All other chemical reagents, including the acyl–coenzyme A:cholesterol acyltransferase inhibitor 58035 (3-[decyldimethylsilyl]-*N*-[2-(4-methylphenyl)-1-phenylethyl] propanamide), were purchased from Sigma-Aldrich unless otherwise specified.

Mice

C57BL6/J WT mice and *Nox2*$^{-/-}$ mice on the C57BL6/J background were purchased from The Jackson Laboratory. *Camk2g*$^{-/-}$ mice on the C57BL6/J background were provided by J. Backs (University of Heidelberg, Heidelberg, Germany) and E. Olson (University of Texas Southwestern Medical Center, Dallas, TX) as described previously (Backs et al., 2010).

Cells

Peritoneal macrophages from WT or mutant mice were harvested 3 d after i.p. injection of concanavalin A or 4 d after i.p. injection of methyl-BSA in mice that had previously been immunized with this antigen (Cook et al., 2003). Macrophages were harvested by peritoneal lavage with ice-cold PBS and maintained in DME containing 10% FBS and 20% L cell–conditioned medium. The medium was replaced every 24 h until the cells reached 80–90% confluency. Cholesterol loading was achieved by incubating the cells with 50 µg/ml acetyl-LDL plus 10 µg/ml 58035 for the indicated times (Devries-Seimon et al., 2005). The medium was changed every other day and immediately before treatments.

Calcium imaging

Macrophages cultured on 25-mm coverslips were placed in 35-mm dishes and loaded with 4 µM Fluo-3 acetoxymethyl ester (Invitrogen) and 0.08% Pluronic F-127 in HBSS at room temperature for 30 min. The cells were then washed twice with HBSS, incubated in HBSS for an additional 30 min, and then mounted on the stage of an inverted confocal microscope (Live5; Carl Zeiss, Inc.) equipped with a 40× objective. 250 µM sulphinpyrazone was included in all solutions to prevent excretion of the Fluo-3 by the macrophages. To trigger IICR, 10 µM ATP was added directly to the cell culture medium (Charest et al., 1985; Li et al., 2009). In some experiments, 2 µM thapsigargin, a sarco-ER calcium-dependent ATPase inhibitor, was added to assess ER calcium stores at the end of the experiments (Li et al., 2009). Cells were excited using the 488-nm laser line, and images were acquired at 1-s intervals under the time-lapse mode and subsequently analyzed using ImageJ (National Institutes of Health). The data are presented as a ratio of f_{max}/f_0, where f_{max} represents the maximum fluorescence intensity obtained with ATP stimulation and f_0 indicates the baseline fluorescence intensity. These data were quantified as area under the curve of the increment in f_{max}/f_0.

Apoptosis assays

Apoptosis was assayed by annexin V staining using an apoptosis assay kit (Vybrant Apoptosis Assay kit #2; Invitrogen) and by TUNEL staining using the In Situ Cell Death Detection kit, tetramethylrhodamine (TMR) red (Roche; Yao and Tabas, 2000). For annexin V, the cells were gently washed once with PBS and then incubated for 15 min at room temperature with 110 µl annexin-binding buffer (25 mM Hepes, 140 mM NaCl, 1 mM EDTA, pH 7.4, and 0.1% BSA) containing 10 µl Alexa Fluor 488– or 594–conjugated annexin V. The staining mixture was removed and replaced with 110 µl of binding buffer. The cells were viewed immediately at room temperature with an inverted fluorescent microscope (IX-70; Olympus) equipped with filters appropriate for fluorescein (Alexa Fluor 488) or rhodamine (Alexa Fluor 594). Images were obtained with a charge-coupled device camera (Cool Snap; Photometrics) equipped with imaging software obtained from Roper Industries. Three fields of ∼700 cells per field were photographed for each condition, and the number of annexin V–positive cells in each field was counted and expressed as a percentage of the total number of cells. TUNEL staining was assayed using

the In Situ Cell Death Detection kit, TMR red. At the end of the incubation period, the cells were gently washed once with PBS and then fixed in 4% paraformaldehyde in PBS for 1 h at room temperature. Then the cells were rinsed once with PBS and permeabilized in 0.1% Triton X-100 with 0.1% sodium citrate for 2 min on ice. The cells were then rinsed twice with PBS, 100 µl TUNEL reaction mixture (10 µl of labeling solution and 90 µl of enzyme solution) was added, and the cells were incubated for 1 h at 37°C with 5% CO_2. The staining mixture was then removed, and the cells were washed three times with PBS and then incubated in fresh PBS. The cells were viewed immediately at room temperature, as for the aforementioned annexin V assay, using filters appropriate for TMR (rhodamine). 10 fields of ~100 cells per field were photographed for each condition, and the number of TUNEL-positive cells in each field was counted and expressed as a percentage of the total number of cells.

Fluorescent analysis of peroxide accumulation
After incubation under control or cholesterol-loading conditions, macrophages were loaded with 5-(and-6)-chloromethyl-2′7′-DCF diacetate acetyl ester (Invitrogen). After 30 min, the cells were washed and viewed immediately at room temperature with an inverted fluorescent microscope (IX-70) equipped with filters appropriate for fluorescein, and images were obtained with a charge-coupled device camera (Cool Snap) equipped with imaging software. Three fields of ~700 cells per field were photographed for each condition, and the number of DCF-positive cells in each field was counted and expressed as a percentage of the total number of cells.

Immunoblotting
Cell extracts were electrophoresed on 4–20% gradient SDS-PAGE gels (Bio-Rad Laboratories) and transferred to 0.22-µM nitrocellulose membranes. The membranes were blocked for 1 h at room temperature in Tris-buffered saline and 0.1% Tween 20 (TBST) containing 5% (wt/vol) nonfat milk. The membranes were then incubated with primary antibody in TBST containing 5% nonfat milk or BSA at 4°C overnight, followed by incubation with the appropriate secondary antibody coupled to horseradish peroxidase. Proteins were detected by ECL (Thermo Fisher Scientific). Anti-CHOP and anti-ATF4 antibodies were obtained from Santa Cruz Biotechnology, Inc.; anti–α-actin, anti–phospho-Thr287-CaMKII, and anti–phospho-PKR antibodies were purchased from Millipore; and anti–phospho-PERK and anti–glyceraldehyde 3-phosphate dehydrogenase (GAPDH) antibodies were obtained from Cell Signaling Technology.

siRNA-mediated gene silencing
siRNAs against murine *Nox2* (SI02686327) and murine *Pkr* (SI01389108) were purchased from QIAGEN. For CaMKII-γ silencing (Fig. 1 D), two *Camk2g* siRNAs were used as described previously (Timmins et al., 2009); *Camk2g* siRNA #1 and *Camk2g* siRNA #2 in Fig. 1 D represent the siRNAs referred to as siRNA 2 and siRNA 3, respectively, in this previous study. For IP3R1 and ERO1α silencing, *Ip3r1* siRNA #1 and *Ero1a* siRNA #3 were used as described previously (Li et al., 2009). Macrophages grown to 50% confluency were transfected with each siRNA using Lipofectamine 2000 (Invitrogen) and 10 pmol siRNA per square centimeter well area (~40,000 macrophages per well in 48-well plates) according to the manufacturer's instructions. After 4 h of transfection, the media were replaced, and, 72 h later, the indicated experiments were conducted.

In vivo model of ER stress using i.p. injection of tunicamycin
C57BL6/J and *Nox2*$^{-/-}$ mice were injected i.p. with concanavalin A, and then, 3 d later, the mice were given an i.p. injection of tunicamycin at a dose of 1 mg/kg of body weight. After 40 h, the kidney was harvested, and cryosections were prepared. TUNEL staining was performed using the In Situ Cell Death Detection kit, TMR red, followed by nuclear counterstaining with DAPI. Sections were mounted with antifade reagent (ProLong Gold; Invitrogen), and images were captured using an inverted microscope (IX-70).

Mitochondrial calcium uptake
Macrophages in phenol red–free medium were incubated on ice for 1 h on a rocking platform with 10 µM Rhod-2–AM (Invitrogen) 4 h before the end of the experiment. The cells were then washed one time with PBS, followed by incubation with the indicated experimental treatment media for 3 h at 37°C. The cells were then imaged using a scanning confocal microscope (LSM 510 META; Carl Zeiss, Inc.) equipped with a 40×/1.3 numerical aperture oil immersion lens. The optical sections were estimated to be 1 µM in thickness. The cells were excited using a 543-nm helium neon laser, and emission fluorescence was detected through a 530-nm long-pass filter. Quantification of the rhodamine signal was conducted using the ImageJ version 1.37v. Intensity values represent the mean integrated fluorescence signal per cell.

Mitochondrial membrane potential
At the end of the indicated treatment periods, macrophages on glass-bottom 35-mm culture dishes (MatTek) were washed two times with PBS and then stained with 100 µM MitoTracker red CMXRos (Invitrogen) for 15–30 min at 37°C. Fluorescent images were captured and quantified as detailed in Mitochondrial calcium uptake for the Rhod-2 method.

Laser capture microdissection and RT-QPCR
RNA from nonendothelial intimal cells was captured by laser capture microdissection using a laser microdissection system (PALM; Carl Zeiss, Inc.). Immunohistochemistry performed on sections that were separated by 6 µm from the captured sections revealed that >70% of the intimal cells were F4/80-positive macrophages. Total RNA was isolated using the RNAqueous-Micro kit (Applied Biosystems) and reverse transcribed into cDNA using SuperScript III First-Strand Synthesis SuperMix (Invitrogen). QPCR was performed as described previously (Feng et al., 2003a).

Immunohistochemistry and immunofluorescence analyses
Mouse kidneys were immersion fixed in 10% neutral-buffered formalin overnight followed by embedding in paraffin. 5-µm paraffin-embedded sections were immunostained using anti-NOX2 antibody (Santa Cruz Biotechnology, Inc.) and the rabbit staining system (ImmunoCruz; Santa Cruz Biotechnology, Inc.). Sections were counterstained with DAPI and mounted with antifade reagent (ProLong Gold). Images were captured using an inverted microscope (Axiovert 200M; Carl Zeiss, Inc.). For immunofluorescence detection of superoxide, the frozen kidney or aorta sections were incubated with 2 µM DHE for 30 min at 37°C and then washed for 5 min with PBS. Sections were counterstained with DAPI and mounted with antifade reagent (ProLong Gold). DHE is a hydrophobic uncharged compound that can cross intracellular membranes and binds to superoxide, which can be monitored as a bright red fluorescence (Laurindo et al., 2008).

Renal function tests
Serum was collected after centrifuging clotted blood at 3,000 *g* for 20 min. The creatinine concentration in serum was measured using a commercially available kit (Creatinine Enzymatic Assay kit; Bio-quant, Inc.). The albumin concentration in the urine was measured by a competitive ELISA (Exocell) and normalized to urine creatinine levels, which were measured as using the Creatinine Enzymatic Assay kit.

Statistics
Data are presented as means ± SEM. For most of the bar graph data, $n = 3$ for each experimental group. However, for the bar graphs depicting f_{max}/f_0 data, n = ~30 per group. Analysis of variance followed by Tukey post-test (Prism 4 version 4.03; GraphPad Software, Inc.) was used to determine statistical significance among all groups. Bars with the same symbols are not significantly different from each other, whereas bars with different symbols are significantly different from each other. P-values for statistically different values ranged from $P < 0.05$ to $P < 0.0001$.

We thank Dr. J. Timmins for assistance with the mitochondrial calcium uptake experiments; G. Kuriakose for technical support; Drs. A. Marks and M.J. Betzenhauser for advice regarding IICR measurements; and Drs. J. Backs and E. Olson for supplying the *Camk2g*$^{-/-}$ mice.

This work was supported by National Institutes of Health grants 5T32HL087745-04 (Multidisciplinary Training in Translational Cardiovascular Research) to C. Scull and HL087123 and HL075662 to I. Tabas.

Submitted: 21 June 2010
Accepted: 8 November 2010

References

Backs, J., P. Stein, T. Backs, F.E. Duncan, C.E. Grueter, J. McAnally, X. Qi, R.M. Schultz, and E.N. Olson. 2010. The gamma isoform of CaM kinase II controls mouse egg activation by regulating cell cycle resumption. *Proc. Natl. Acad. Sci. USA.* 107:81–86. doi:10.1073/pnas.0912658106

Barry-Lane, P.A., C. Patterson, M. van der Merwe, Z. Hu, S.M. Holland, E.T. Yeh, and M.S. Runge. 2001. p47phox is required for atherosclerotic lesion progression in ApoE(−/−) mice. *J. Clin. Invest.* 108: 1513–1522.

Basu, S.K., J.L. Goldstein, G.W. Anderson, and M.S. Brown. 1976. Degradation of cationized low density lipoprotein and regulation of cholesterol metabolism in homozygous familial hypercholesterolemia fibroblasts. *Proc. Natl. Acad. Sci. USA.* 73:3178–3182. doi:10.1073/pnas.73.9.3178

Bonomini, F., S. Tengattini, A. Fabiano, R. Bianchi, and R. Rezzani. 2008. Atherosclerosis and oxidative stress. *Histol. Histopathol.* 23:381–390.

Chandra, J., A. Samali, and S. Orrenius. 2000. Triggering and modulation of apoptosis by oxidative stress. *Free Radic. Biol. Med.* 29:323–333.

Charest, R., P.F. Blackmore, and J.H. Exton. 1985. Characterization of responses of isolated rat hepatocytes to ATP and ADP. *J. Biol. Chem.* 260:15789–15794.

Cook, A.D., E.L. Braine, and J.A. Hamilton. 2003. The phenotype of inflammatory macrophages is stimulus dependent: implications for the nature of the inflammatory response. *J. Immunol.* 171:4816–4823.

Devries-Seimon, T., Y. Li, P.M. Yao, E. Stone, Y. Wang, R.J. Davis, R. Flavell, and I. Tabas. 2005. Cholesterol-induced macrophage apoptosis requires ER stress pathways and engagement of the type A scavenger receptor. *J. Cell Biol.* 171:61–73. doi:10.1083/jcb.200502078

Feng, B., P.M. Yao, Y. Li, C.M. Devlin, D. Zhang, H.P. Harding, M. Sweeney, J.X. Rong, G. Kuriakose, E.A. Fisher, et al. 2003a. The endoplasmic reticulum is the site of cholesterol-induced cytotoxicity in macrophages. *Nat. Cell Biol.* 5:781–792. doi:10.1038/ncb1035

Feng, B., D. Zhang, G. Kuriakose, C.M. Devlin, M. Kockx, and I. Tabas. 2003b. Niemann-Pick C heterozygosity confers resistance to lesional necrosis and macrophage apoptosis in murine atherosclerosis. *Proc. Natl. Acad. Sci. USA.* 100:10423–10428.

Forman, H.J., and M. Torres. 2002. Reactive oxygen species and cell signaling: respiratory burst in macrophage signaling. *Am. J. Respir. Crit. Care Med.* 166:S4–S8.

Furukawa, S., T. Fujita, M. Shimabukuro, M. Iwaki, Y. Yamada, Y. Nakajima, O. Nakayama, M. Makishima, M. Matsuda, and I. Shimomura. 2004. Increased oxidative stress in obesity and its impact on metabolic syndrome. *J. Clin. Invest.* 114:1752–1761.

Glass, C.K., and J.L. Witztum. 2001. Atherosclerosis. the road ahead. *Cell.* 104:503–516. doi:10.1016/S0092-8674(01)00238-0

Green, D.R., and J.C. Reed. 1998. Mitochondria and apoptosis. *Science.* 281: 1309–1312. doi:10.1126/science.281.5381.1309

Havel, R.J., H.A. Eder, and J.H. Bragdon. 1955. The distribution and chemical composition of ultracentrifugally separated lipoproteins in human serum. *J. Clin. Invest.* 34:1345–1353.

Healy, S.J., A.M. Gorman, P. Mousavi-Shafaei, S. Gupta, and A. Samali. 2009. Targeting the endoplasmic reticulum-stress response as an anticancer strategy. *Eur. J. Pharmacol.* 625:234–246.

Hsich, E., B.H. Segal, P.J. Pagano, F.E. Rey, B. Paigen, J. Deleonardis, R.F. Hoyt, S.M. Holland, and T. Finkel. 2000. Vascular effects following homozygous disruption of p47(phox): an essential component of NADPH oxidase. *Circulation.* 101:1234–1236.

Ibrahimi, A., and N.A. Abumrad. 2002. Role of CD36 in membrane transport of long-chain fatty acids. *Curr. Opin. Clin. Nutr. Metab. Care.* 5:139–145. doi:10.1097/00075197-200203000-00004

Iles, K.E., and H.J. Forman. 2002. Macrophage signaling and respiratory burst. *Immunol. Res.* 26:95–105. doi:10.1385/IR:26:1-3:095

Judkins, C.P., H. Diep, B.R. Broughton, A.E. Mast, E.U. Hooker, A.A. Miller, S. Selemidis, G.J. Dusting, C.G. Sobey, and G.R. Drummond. 2010. Direct evidence of a role for Nox2 in superoxide production, reduced nitric oxide bioavailability, and early atherosclerotic plaque formation in ApoE−/− mice. *Am. J. Physiol. Heart Circ. Physiol.* 298:H24–H32.

Kim, I., W. Xu, and J.C. Reed. 2008. Cell death and endoplasmic reticulum stress: disease relevance and therapeutic opportunities. *Nat. Rev. Drug Discov.* 7:1013–1030.

Kirk, E.A., M.C. Dinauer, H. Rosen, A. Chait, J.W. Heinecke, and R.C. LeBoeuf. 2000. Impaired superoxide production due to a deficiency in phagocyte NADPH oxidase fails to inhibit atherosclerosis in mice. *Arterioscler. Thromb. Vasc. Biol.* 20:1529–1535.

Kitamura, M. 2008. Endoplasmic reticulum stress in the kidney. *Clin. Exp. Nephrol.* 12:317–325. doi:10.1007/s10157-008-0060-7

Kregel, K.C., and H.J. Zhang. 2007. An integrated view of oxidative stress in aging: basic mechanisms, functional effects, and pathological considerations. *Am. J. Physiol. Regul. Integr. Comp. Physiol.* 292:R18–R36.

Kris-Etherton, P.M., A.H. Lichtenstein, B.V. Howard, D. Steinberg, and J.L. Witztum; Nutrition Committee of the American Heart Association Council on Nutrition, Physical Activity, and Metabolism. 2004. Antioxidant vitamin supplements and cardiovascular disease. *Circulation.* 110:637–641.

Laurindo, F.R., D.C. Fernandes, and C.X. Santos. 2008. Assessment of superoxide production and NADPH oxidase activity by HPLC analysis of dihydroethidium oxidation products. *Methods Enzymol.* 441:237–260.

Lee, E.S., C.H. Yoon, Y.S. Kim, and Y.S. Bae. 2007. The double-strand RNA-dependent protein kinase PKR plays a significant role in a sustained ER stress-induced apoptosis. *FEBS Lett.* 581:4325–4332. doi:10.1016/j.febslet.2007.08.001

Li, G., M. Mongillo, K.T. Chin, H. Harding, D. Ron, A.R. Marks, and I. Tabas. 2009. Role of ERO1-α–mediated stimulation of inositol 1,4,5-triphosphate receptor activity in endoplasmic reticulum stress–induced apoptosis. *J. Cell Biol.* 186:783–792. doi:10.1083/jcb.200904060

Locatelli, F., B. Canaud, K.U. Eckardt, P. Stenvinkel, C. Wanner, and C. Zoccali. 2003. Oxidative stress in end-stage renal disease: an emerging threat to patient outcome. *Nephrol. Dial. Transplant.* 18:1272–1280. doi:10.1093/ndt/gfg074

Malhotra, J.D., and R.J. Kaufman. 2007a. Endoplasmic reticulum stress and oxidative stress: a vicious cycle or a double-edged sword? *Antioxid. Redox Signal.* 9:2277–2293.

Malhotra, J.D., and R.J. Kaufman. 2007b. The endoplasmic reticulum and the unfolded protein response. *Semin. Cell Dev. Biol.* 18:716–731.

Martínez, J.A. 2006. Mitochondrial oxidative stress and inflammation: an slalom to obesity and insulin resistance. *J. Physiol. Biochem.* 62:303–306. doi:10.1007/BF03165759

Myoishi, M., H. Hao, T. Minamino, K. Watanabe, K. Nishihira, K. Hatakeyama, Y. Asada, K. Okada, H. Ishibashi-Ueda, G. Gabbiani, et al. 2007. Increased endoplasmic reticulum stress in atherosclerotic plaques associated with acute coronary syndrome. *Circulation.* 116:1226–1233. doi:10.1161/CIRCULATIONAHA.106.682054

Nakamura, T., M. Furuhashi, P. Li, H. Cao, G. Tuncman, N. Sonenberg, C.Z. Gorgun, and G.S. Hotamisligil. 2010. Double-stranded RNA-dependent protein kinase links pathogen sensing with stress and metabolic homeostasis. *Cell.* 140:338–348. doi:10.1016/j.cell.2010.01.001

Pedruzzi, E., C. Guichard, V. Ollivier, F. Driss, M. Fay, C. Prunet, J.C. Marie, C. Pouzet, M. Samadi, C. Elbim, et al. 2004. NAD(P)H oxidase Nox-4 mediates 7-ketocholesterol-induced endoplasmic reticulum stress and apoptosis in human aortic smooth muscle cells. *Mol. Cell. Biol.* 24: 10703–10717.

Pollock, J.D., D.A. Williams, M.A. Gifford, L.L. Li, X. Du, J. Fisherman, S.H. Orkin, C.M. Doerschuk, and M.C. Dinauer. 1995. Mouse model of X-linked chronic granulomatous disease, an inherited defect in phagocyte superoxide production. *Nat. Genet.* 9:202–209.

Poot, M., Y.Z. Zhang, J.A. Krämer, K.S. Wells, L.J. Jones, D.K. Hanzel, A.G. Lugade, V.L. Singer, and R.P. Haugland. 1996. Analysis of mitochondrial morphology and function with novel fixable fluorescent stains. *J. Histochem. Cytochem.* 44:1363–1372.

Pyo, C.W., S.H. Lee, and S.Y. Choi. 2008. Oxidative stress induces PKR-dependent apoptosis via IFN-gamma activation signaling in Jurkat T cells. *Biochem. Biophys. Res. Commun.* 377:1001–1006. doi:10.1016/j.bbrc.2008.10.103

Ron, D., and P. Walter. 2007. Signal integration in the endoplasmic reticulum unfolded protein response. *Nat. Rev. Mol. Cell Biol.* 8:519–529. doi:10.1038/nrm2199

Sorescu, D., D. Weiss, B. Lassègue, R.E. Clempus, K. Szöcs, G.P. Sorescu, L. Valppu, M.T. Quinn, J.D. Lambeth, J.D. Vega, et al. 2002. Superoxide production and expression of nox family proteins in human atherosclerosis. *Circulation.* 105:1429–1435.

Tabas, I. 2002. Consequences of cellular cholesterol accumulation: basic concepts and physiological implications. *J. Clin. Invest.* 110:905–911.

Tabas, I. 2010. The role of endoplasmic reticulum stress in the progression of atherosclerosis. *Circ. Res.* 107:839–850.

Thorp, E., G. Li, T.A. Seimon, G. Kuriakose, D. Ron, and I. Tabas. 2009. Reduced apoptosis and plaque necrosis in advanced atherosclerotic lesions of *Apoe*−/− and *Ldlr*−/− mice lacking CHOP. *Cell Metab.* 9:474–481. doi:10.1016/j.cmet.2009.03.003

Timmins, J.M., L. Ozcan, T.A. Seimon, G. Li, C. Malagelada, J. Backs, T. Backs, R. Bassel-Duby, E.N. Olson, M.E. Anderson, and I. Tabas. 2009. Calcium/calmodulin-dependent protein kinase II links ER stress with Fas and mitochondrial apoptosis pathways. *J. Clin. Invest.* 119:2925–2941. doi:10.1172/JCI38857

Trollinger, D.R., W.E. Cascio, and J.J. Lemasters. 1997. Selective loading of Rhod 2 into mitochondria shows mitochondrial Ca2+ transients during the contractile cycle in adult rabbit cardiac myocytes. *Biochem. Biophys. Res. Commun.* 236:738–742.

Vendrov, A.E., Z.S. Hakim, N.R. Madamanchi, M. Rojas, C. Madamanchi, and M.S. Runge. 2007. Atherosclerosis is attenuated by limiting superoxide generation in both macrophages and vessel wall cells. *Arterioscler. Thromb. Vasc. Biol.* 27:2714–2721.

Verrax, J., R.C. Pedrosa, R. Beck, N. Dejeans, H. Taper, and P.B. Calderon. 2009. In situ modulation of oxidative stress: a novel and efficient strategy to kill cancer cells. *Curr. Med. Chem.* 16:1821–1830. doi:10.2174/092986709788186057

Williams, K.J., and E.A. Fisher. 2005. Oxidation, lipoproteins, and atherosclerosis: which is wrong, the antioxidants or the theory? *Curr. Opin. Clin. Nutr. Metab. Care.* 8:139–146. doi:10.1097/00075197-200503000-00006

Wolber, R.A., R.E. Duque, J.P. Robinson, and H.A. Oberman. 1987. Oxidative product formation in irradiated neutrophils. A flow cytometric analysis. *Transfusion.* 27:167–170. doi:10.1046/j.1537-2995.1987.27287150192.x

Yao, P.M., and I. Tabas. 2000. Free cholesterol loading of macrophages induces apoptosis involving the fas pathway. *J. Biol. Chem.* 275:23807–23813.

Yao, P.M., and I. Tabas. 2001. Free cholesterol loading of macrophages is associated with widespread mitochondrial dysfunction and activation of the mitochondrial apoptosis pathway. *J. Biol. Chem.* 276:42468–42476.

Zinszner, H., M. Kuroda, X. Wang, N. Batchvarova, R.T. Lightfoot, H. Remotti, J.L. Stevens, and D. Ron. 1998. CHOP is implicated in programmed cell death in response to impaired function of the endoplasmic reticulum. *Genes Dev.* 12:982–995. doi:10.1101/gad.12.7.982